Supplementary Material for paper 'Threshold shear stress for the transition between tumbling and tank-treading of red blood cells in shear flow – Dependence on the viscosity of the suspending medium'

By T.M. Fischer and R. Korzeniewski

1 Perfusion system

Figure 1 schematically shows a cross section through the capillary and its embedding. Capillaries were from Hilgenberg GmbH (Malsfeld, Germany). The dimensions were: wall thickness = 24 μm, based on electron microscopy of a capillary of the same batch as the one used in the experiments, inner diameter = 975 μm as determined by light microscopy, and length = 30 mm. At both ends, the capillary was held by an aluminum support and connected with large bore silicone tubing to stainless steel tubes glued to the aluminum support. This setting minimized mechanical disturbance of the thin walled capillary during the experiments and during the subsequent cleaning procedure so that all experiments could be made with the same capillary. The solution outside the capillary had the same refractive index as the solution which was used for perfusion.

The perfusion was driven by constant pressure from an air filled reservoir containing 10 ℓ. The reservoir was pressurized up to 125 mm Hg using a pump with large bore tubing to avoid heating of the compressed air. A tight filling of the reservoir with 900g aluminum turnings also stabilized the temperature due to the high heat capacity of aluminum. The pressure was stable for several hours without flow. The pressure in the reservoir was applied to the free surface of the suspension contained in a vial from where it flowed via tubing to the stainless steel tubes glued to the aluminum support of the capillary (see above).

To vary the flow rate, various cannulas were connected to the outflow of the capillary. Special attention had to be paid in order to avoid droplets being formed at the tip of the cannulas during flow, because the separation of a droplet from the tip caused a sudden transient in flow velocity. Slow variations of flow velocity, however, did occur for unknown reasons. These variations did not matter because the current flow velocity was measured and used to calculate the shear rate.

2 Microscopic imaging and registration

The aluminum support of the capillary was fastened to the stage of an ACM upright microscope (Zeiss, Göttingen, Germany). The flow of suspended particles

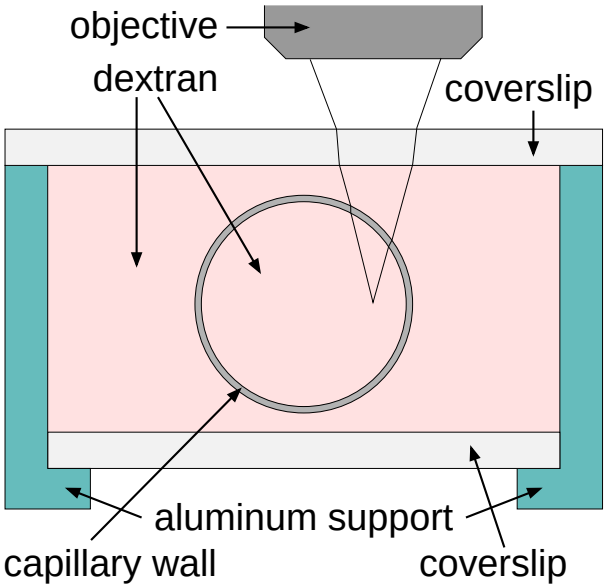

Figure 1: Schematic cross section of the embedding of the glass capillary. The magnification and the numerical aperture of the objective are 16 and 0.35, respectively.

or red cells was observed in bright field using a 16x objective with 0.35 numerical aperture. Illumination was performed with a green LED (Luxeon V, Philips) adapted to the original lamp house to illuminate exactly the back focal plane of the condensor. The wavelength (415 nm) corresponds to a local maximum in the absorption of hemoglobin. To avoid motion blurr, a flash of 32 μs duration was used, which essentially freezes velocities up to 16 mm/s. The microscopic image was recorded with a b/w interlaced CCD camera (jai, M-50, Stemmer Imaging, Puchheim, Germany). The short edge of the frame was oriented parallel to the capillary wall. The film scenes were recorded on video tape (DV, Digital Video Casette) and simultaneously saved on the hard disc of a computer using the free software kino (http://www.kinodv.org/).

In principle, measuring the velocity of fast moving objects from TV movies is limited by the frequency of half frames; i.e. in Europe 50/s. This limitation was overcome by driving the flash illumination (KHS Electronics u. Laborgeräte, Aachen, Germany) with unequal intervals (1). The intervals used for the measurement of velocity ranged from 0.63 ms to 38 ms.

The radial range of the microscopic image covers 162 μm. The calculation of radial positions within the image is based on a calibration of pixel size with a stage micrometer. The position of the microscope stage in radial direction was measured to submicron sensitivity with an inductive probe (Mahr GmbH, Göttingen, Germany). For the experiments in section 4 the position parallel to the optical axis was

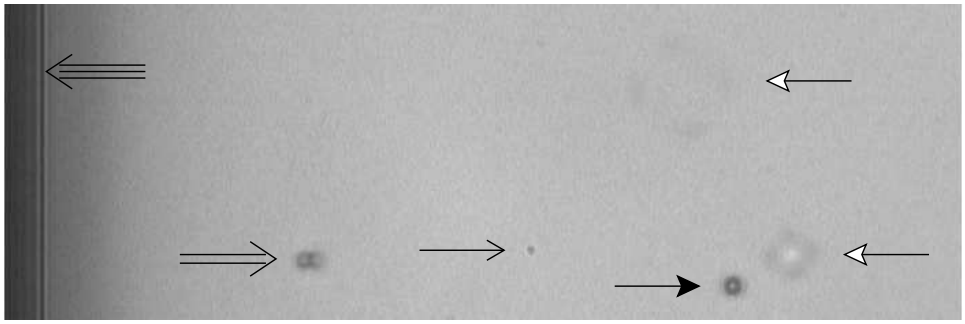

Figure 2: Completed image of a half frame showing latex spheres (diameter 2.03 μm) flowing in the capillary. The latex spheres were suspended in dextran solution. The flow direction is vertical. The centerline of the capillary is outside of this image. Black arrowhead: in focus. Double lined arrow: moderately out of focus. White arrowheads: strongly out of focus. Single lined arrow with open arrowhead: dust on the glass plate covering the CCD chip. Triple lined arrow: capillary wall. The width of the image corresponds to 162 μm.

measured with an inductive probe of the same type.

The image of the objects in focus was not visibly distorted (Figure 2). However, objects not in focus were not just blurred but in addition split up in radial direction or in radial plus flow direction, respectively, into two or four blurred images. This splitting became particularly apparent with small objects (Figure 2). A moderate splitting in radial direction is also evident in Figure 3d at the lower end of the red cell where the contour has negative curvature.

3 Processing of the microscopic images

Offline evaluation of the microscopic images was performed under linux. The code was written in python. The following steps were performed sequentially.

1. The recorded scenes, one for each outflow resistance, were split into single uncompressed images (.pgm) using the free software mplayer (http://www.mplayerhq.hu/design7/news.html). In these single images, the pixels were no more exactly square shaped (see the black stripes to both sides in Fig. 3a. The distortion was accounted for when θ, L, and D were calculated. Each of the two half frames comprising an image was completed to a full frame by filling the empty lines via linear interpolation of the grey scale values (GVs) of the adjacent lines.

2. The GVs of all images were corrected using an empty image containing no

red cells according to:

$$\mathrm{GV}_{\mathrm{corrected}} = \frac{\mathrm{GV}_{\mathrm{image}} \cdot 255}{\mathrm{GV}_{\mathrm{empty\,image}}}. \quad (1)$$

Because of noise, Equation 1 results in $\mathrm{GV}_{\mathrm{corrected}} > 255$ for some background pixels. In such cases $\mathrm{GV}_{\mathrm{corrected}}$ was set equal to 255. The correction of GVs was necessary because towards the capillary wall the background was darker than in the middle (Figure 2). As a welcome side effect of the correction (Equation 1), there was no interference of dust on the glass plate covering the CCD chip (Figure 3a, c, d) with the image processing.

3. The corrected images were converted into binary images using a threshold in GV. Its value was chosen to maximize the average gradient (QF, see below) in GV on the contour (determination see below) as judged from the histograms of GVs. This conversion resulted in black objects on white background.

4. The binary images were scanned for objects. The shape of an object was determined by finding its contour. A strategy was devised, which accepted a black pixel as belonging to the object only when the pixel in question had at least one edge in common with the rest of the object. This way, black pixels which adhered to each other solely via their vertices belonged to two different objects (Figure 3b). Objects with their contour touching the rim of the image were excluded except for the check of close proximity (see below). The completed image of a tank-treading red cell is shown in Figure 3c. The contour overlaid on the same image is shown in Figure 3d with black pixels.

5. Three different areas of each object were evaluated. A) The number of black pixels inside and including the contour. B) Area A plus any white pixels inside the contour. C) Area B plus any white pixels in each line between the outermost contour pixels at right angles to the flow direction. The cell shown in Figure 3c and d is an example for $\mathrm{B} < \mathrm{C}$. Such cells were accepted provided $\mathrm{B}/\mathrm{C} > 0.985$.

   The center of objects was calculated from the pixels constituting area B. Small objects were excluded by threshold values in minimum area B and minimum contour length. The value for minimum area depended weakly in a linear fashion on L. Overlapping cells were recognized as single objects. They were excluded by a threshold value in maximum area B.

6. The orientation of deformed objects with respect to the flow direction was obtained by determination of the principal axes of the moment of inertia of area B. The lengths of major and minor half axes were defined as the distance from the center of the objects to the intersection of the principal axes with the outer edge of the contour. The sum of the two major half axes is called L and accordingly D for the two minor ones. L and D are shown in Figure 3d

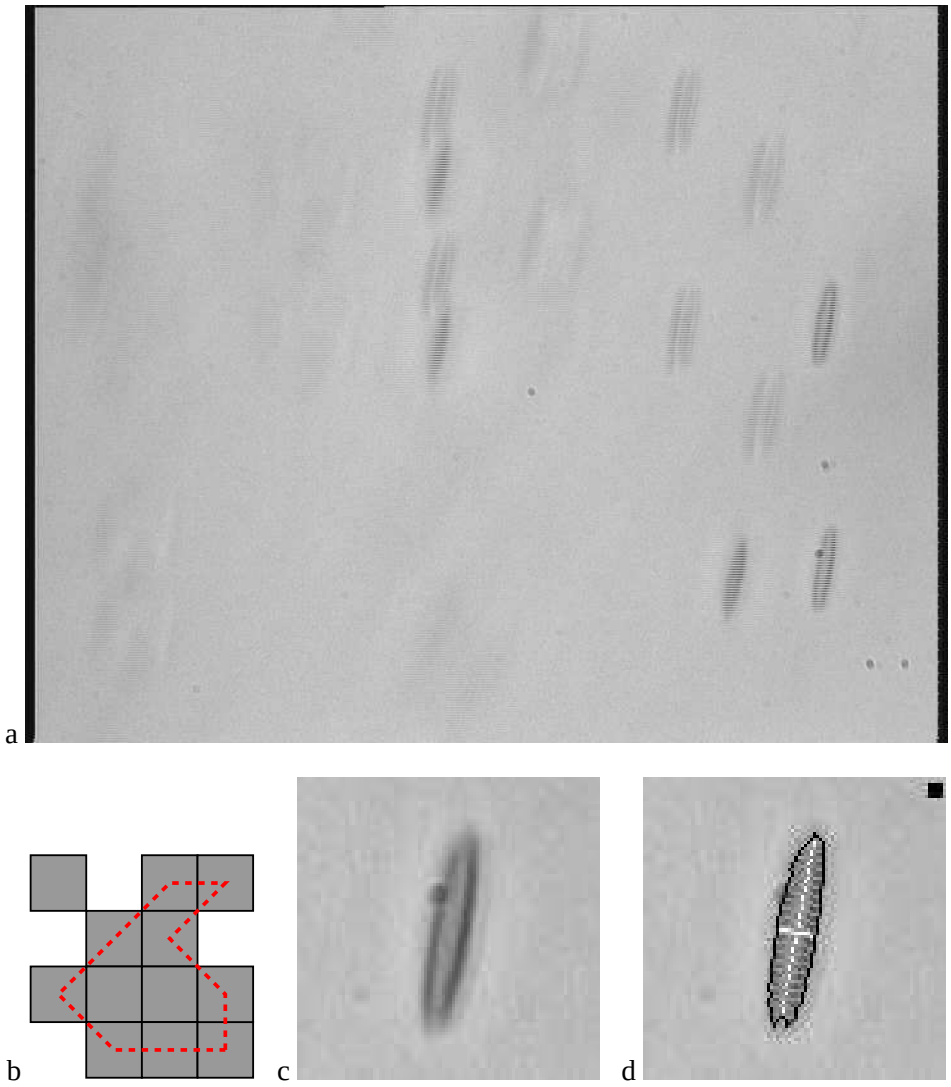

Figure 3: Image processing of red cells. a: Full frame showing red cells suspended in dextran-salt solution of 23.9 mPas and subjected to a shear flow of 120/s on average. The width of the frame corresponds to 162 μm. The interval between the flashes exposing the same cell in each half frame was xx ms. b: Schematic of the contour finding process. The upper left pixel does not belong to the object whose contour is defined by the dashed line. c: Completed image of the lower one of the two rightmost red cells in a. The width of the image corresponds to 23.1 μm. d: Same image as c but overlaid with the major and minor axes (white), then with the subaxes (grey), and finally with the contour (black). Area B/area C = 0.9892 (see text for details). The flow direction in a, c, and d is vertical and the capillary wall is at the left hand side. The circular spots are due to dust on the glass plate covering the CCD chip.

with white pixels. They do not extend all the way onto the contour because the contour was overlaid onto the picture after the axes.

7. The four pixels having an edge in common with a pixel of the contour (labelled top, bottom, left, and right) were used to calculate the absolute value ($\mathrm{g_p}$) of the local gradient in GV.

$$\mathrm{g_p} = \sqrt{(\mathrm{GV_{left}} - \mathrm{GV_{right}})^2 + (\mathrm{GV_{top}} - \mathrm{GV_{bottom}})^2}, \qquad (2)$$

where the GVs were taken from the background-corrected images. The averaged value of $\mathrm{g_p}$ served as a measure of the quality of the focus (QF) of the particular object.

$$\mathrm{QF} = \sum_{\mathrm{p}=1}^{\mathrm{n}} \mathrm{g_p}, \qquad (3)$$

where n was the number of pixels of the contour. QF was used twofold. First, histograms of QF served as a criterion to choose the value of the threshold in GV (see above). Second, by applying an appropriate threshold QF served to exclude TT cells not in focus or TB red cells not oriented edge-on even when they are in focus (see Figure 4).

8. To exclude the influence of a fluid dynamical interaction between close objects on their shape and/or orientation, two objects were excluded when both of the following conditions were fulfilled. (i) the centers were closer than 19 μm. (ii) QF of both objects was greater than half the exclusion threshold.

9. To measure the symmetry of objects the length of *sub*axes was calculated. These subaxes were parallel to the minor axis and started at the major axis at distances $1.5\,w + \mathrm{n} \cdot 3\,w$ from the center, where w is the side length of a pixel and n = 0, 1, 2 ... until the end of the object was encountered. The subaxes are shown in Figure 3d with grey pixels.

   Three measures of symmetry were calculated by summing the absolute values of the differences in length of pairs of subaxes. Corresponding pairs were chosen as to determine the mirror symmetry with respect to both principal axes and the symmetry corresponding to a rotation by 180° around the center of the objects. A fourth measure was the absolute value of the difference of the two major half axes.

   Red cells whose shape had become abnormal probably due to the suspension in a non physiological medium were excluded from further evaluation by applying filters with appropriate threshold values of the four symmetry measures. These threshold values depended weakly in a linear fashion on L.

10. The smoothness of the contour was checked in two ways. First, the difference of neighboring subaxes and from these again the difference was calculated. This way, a measure of the local curvature along the contour of red

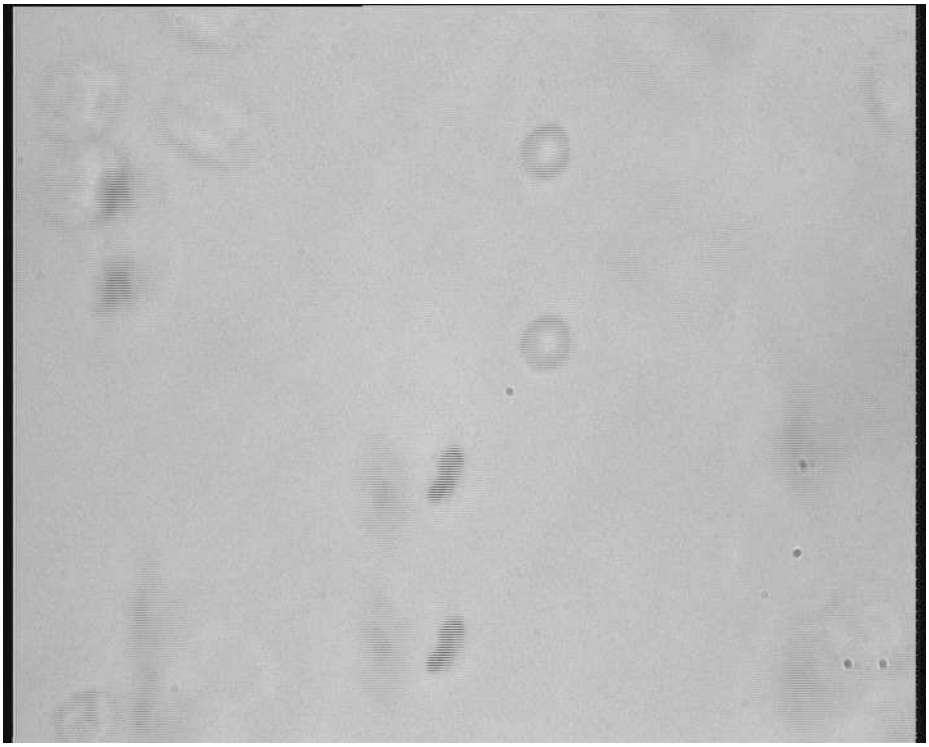

Figure 4: Full frame showing red cells suspended in dextran-salt solution of 10.7 mPas and subjected to a shear flow of 5/s on average. The cells are in the TB regime. Two cells are in focus, one oriented edge-on the other oriented face-on.

cells was obtained. The outermost two subaxes were excluded because cells show strong curvatures at the ends naturally. The maximum and minimum value were used to exclude cells with local outward or inward bulges via threshold values.

Second, the number of pixel pairs juxtaposed at right angles to the flow direction was counted. Only pairs of pixels in the interval $(y_\mathrm{s} - 0.8L_1 cos^2(\theta), y_\mathrm{s} + 0.8L_2 cos^2(\theta))$ were used, where y_s is the y-coordinate of the cell center, L_1 the upper half major axis, L_2 the lower half major axis, and θ the inclination angle. The exponent of two was pragmatically chosen, in order to avoid that with increasing θ the curvature at the cell ends contributes to this sum. With increasing θ, juxtaposed pixel pairs occur not just at the cell ends. Therefore their number was multiplied with cos^3, where the exponent of three was also pragmatically chosen. A threshold value for this modified number of pixel pairs served to exclude cells with strong kinks along their contour.

11. Two images (e.g. Figure 3c, d) of each object which passed the threshold criteria were stored separately. In addition, such pairs of images were stored

for objects having values up to 10% above or below their respective thresholds. This allowed to choose values for the various thresholds that made the percentage of falsely rejected and falsely accepted cells approximately equal, by screening these images.

12. From the distance of the same red cell in the two halves of a full frame and the time interval between the respective flashes, the velocity of flowing objects was calculated (see Figure 3a). The maximum time interval (38ms) was limited by the constant frame rate (25/s). For low velocities, this time interval results in small distances travelled between the two half frames and the recording of the same cell in several consecutive full frames. In these cases, the evaluation of the velocity encompassed as many full frames as possible for each red cell.

4 Experiments to find the proper focus to be used in the experiments

The microscopic image of the inner wall of a capillary was influenced by total reflection at the curved surfaces which separate media of different refractive indices (Figure 5a). In order to know how the image of the wall looks like when the focus was on the capillary midplane, separate experiments were performed.

The capillary was perfused at constant pressure with a suspension of latex spheres (diameter 2.03 μm). During the perfusion, the capillary was moved in radial direction so that alternately one inner wall and the middle of the capillary appeared on the microscopic image. In each of these positions the focus was moved stepwise from safely below to safely above the midplane of the capillary. At each step the position of the objective was read at the vertical inductive probe and a scene of 20 s was recorded. In the middle of the capillary the steps were approximately 8 μm; at the rim the steps were smaller.

From each scene recorded in the middle of the capillary, the velocity of latex spheres in focus was evaluated. The velocities were fitted with a parabola to find the maximal velocity. These maximal velocities depended on the reading of the vertical inductive probe and were again fitted by a parabola. The maximum of this parabola indicated the reading at which the focus was on the midplane of the capillary. The microscopic images of the inner wall depended on the focus. Based on equivalent readings of the vertical inductive probe, the image of the inner wall was found where the focus was on the midplane of the capillary. In the experiments with red cells the focus was set on the midplane of the capillary by reproducing this image of the inner wall (Figure 5a).

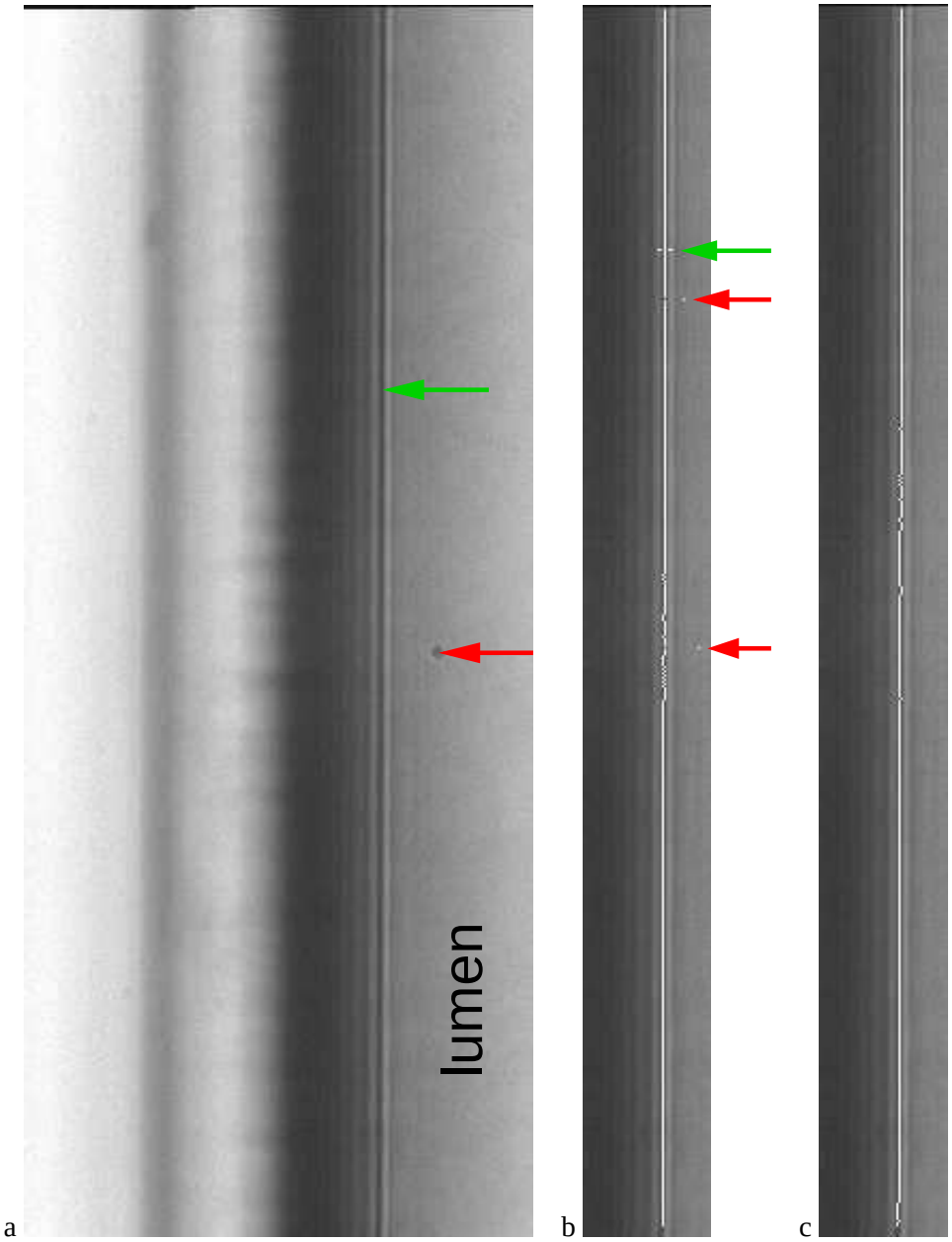

Figure 5: Image processing of the capillary wall. The height of the images corresponds to 122 μm. a: The green arrow points to the black line the position of which was found by image processing. The red arrow points to a spot which is due to dust on the glass plate covering the CCD chip. b: The same image as (a) but more trimmed. The minimum of the second derivative in GVs normal to the wall in each line is indicated by a white pixel. The green arrow points to the absolute minimum of the second derivative. The red arrows point to outliers. c: The final position of the wall (white pixels) as found after elimination of the outliers by execution of the creep routine. See text for details.

5 Determination of the apparent radial position

Each time before testing a new suspension, the microscope stage was moved in radial direction to position the left and right capillary wall approximately in the middle of the microscopic image. In both positions images were taken and the display on the horizontal inductive probe was read. An image trimmed to show basically the capillary wall is shown in Figure 5a. The position of the dark column lined by two lighter columns (green arrow) was evaluated by image processing as follows.

In each line the difference in GV of neighbouring pixels was calculated. This difference is a measure of the first derivative in GV normal to the capillary wall. Repeating this procedure resulted in the second derivative. The pixels with the lowest value of this second derivative are shown in white in Figure 5b. In most cases this minimum was already on the black column or next to it. Sometimes outliers were observed. A typical case is shown in Figure 5b where two white pixels are displaced from the black line (red arrows). To eliminate such outliers, a so called creep routine followed. This routine starts at the white pixel distinguished in Figure 5b by two marks to the left and right hand side (green arrow). This pixel was found as follows: the median of the horizontal position of all white pixels in Figure 5b was determined. Among all white pixels having the same horizontal position as the median, the one with the lowest value of the second derivative was chosen. The creep routine progressed from this pixel in both directions by finding iteratively the lowest GV in the respective adjacent line in the same column or one column to the right or to the left. These pixels (white in Figure 5c) were taken to represent the black line. This procedure worked even when an image was spoiled by an object out of focus (not shown).

A linear regression through these pixels was calculated. The average values of the two slopes were used to correct θ accordingly. The radial position of the two regression lines and the respective readings of the horizontal inductive probe are used to calculate the position of the centerline with respect to the inductive probe. The apparent radial position of individual red cells within the capillary was calculated using their position within the image, the respective reading of the horizontal inductive probe, and the position of the centerline.

6 Theoretical calculation of the surface being in focus

Light rays emanating from a red cell are refracted several times before entering the objective. As a consequence the apparent image of an object is expected to be shifted from its actual position. The situation is depicted in Figure 6a. It shows schematically a cross section through the capillary and two bundles of rays (continuous magenta lines with $\mathrm{aperture} = \sin\alpha$) one focussing the capillary centerline, the other focussing a red cell (red) after moving the objective horizontally offcenter. The blue dashed-dotted lines indicate the respective optical axes. Without

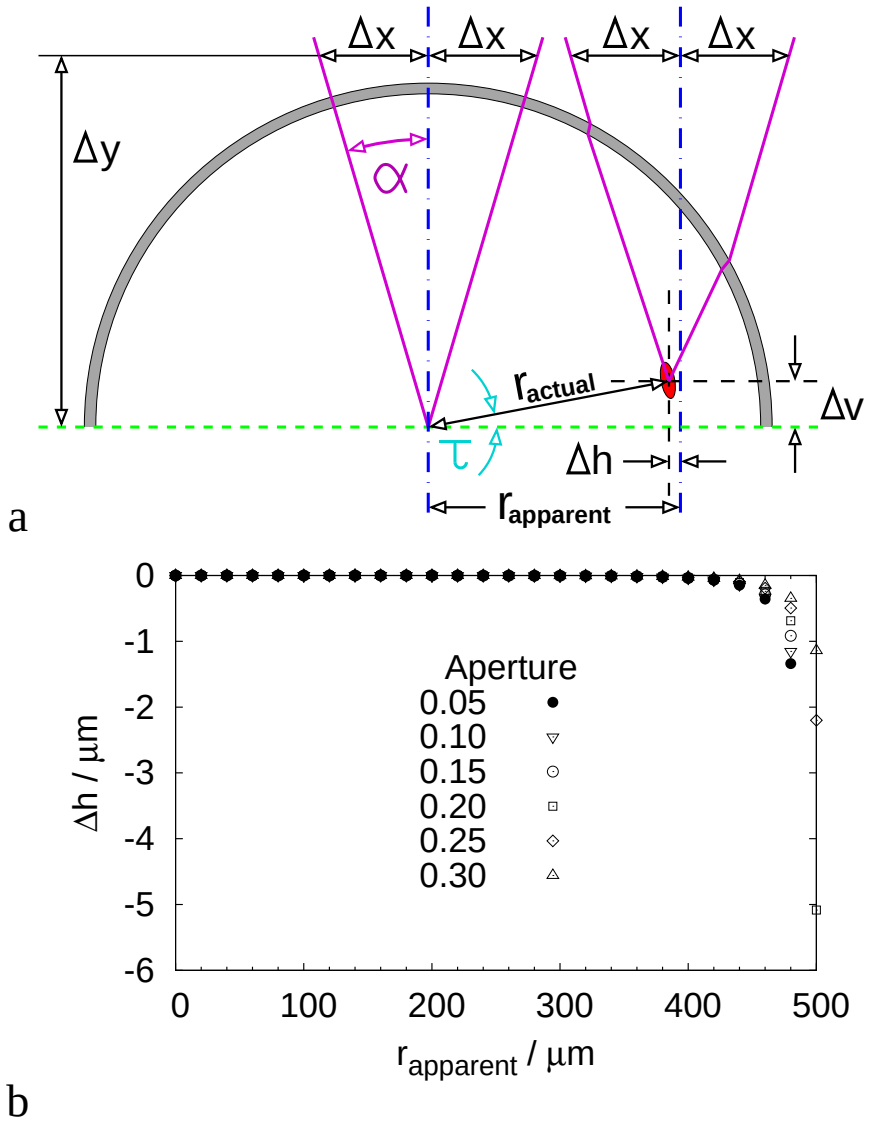

Figure 6: Geometric optics calculation for microscopic imaging through a glass capillary embedded in the same liquid as inside the capillary. The radii were, respectively, 0.492 and 0.516 mm for the inner and outer radius of the capillary. The refractive indices were, respectively, 1.355 and 1.515 for the liquid and glass. a: Schematic cross section through the capillary showing two bundles of rays (continuous magenta lines with $\mathrm{aperture} = \sin\alpha$), one focussing on the capillary centerline, the other focussing a red cell (red) after moving the objective horizontally offcenter. The blue dashed-dotted lines indicate the respective optical axes. b: Horizontal distance (Δh) of the focussed red cell from the optical axis versus the distance of the optical axis from the capillary centerline.

refraction the offcentered bundle of rays would be focussed on the intersection of the optical axis with the capillary midline (green dashed) which is the apparent position of the red cell. The actual position deviates from the apparent one in horizontal (Δh) and vertical direction (Δv). To quantitate these deviations a geometric optics calculation was performed.

First, the case was considered when the optical axis intersects the centerline of the capillary. Here, light rays propagating from the centerline traverse the capillary wall unrefracted (Figure 6a). For numerical apertures ranging from 0.05 to 0.30, two rays starting at the centerline with positive and negative inclination from the optical axis were used to determine their distance (Δx) at an arbitrary but fixed height (Δy) above the capillary but still within the embedding solution.

Second, off center cases were calculated. For each numerical aperture the course of rays starting from the points ($r_{\mathrm{apparent}} \pm \Delta x, \Delta y$) into the capillary with the respective inclinations was calculated. The intersection of the two rays was taken as the actual focus at the respective aperture and at r_{apparent}.

A maximum numerical aperture of 0.30 was used because this is the approximate value after rays of numerical aperture of 0.35, the maximum of the objective, traverse the top coverslip separating two media of different refractive index.

Figures 6b and 7c show the position of the focus versus r_{apparent}. The deviation (Δh) at right angles to the optical axis was very small (Figure 6b). This is due to the fact that the horizontal shift of corresponding rays with positive and negative inclination is opposite. As a consequence of this opposite shift the deviation (Δv) parallel to the optical axis is an order of magnitude higher (Figure 7c). It happened that for the present setting $r_{\mathrm{apparent}}/r_{\mathrm{actual}} - 1 < 10^{-11}$ (data not shown). Therefore r_{apparent} was used instead of r_{actual} in evaluating the data.

As a consequence of the elevation of the actual focus above the midplane of the capillary, red cells tank-treading are oriented not exactly edge on. The tilt angle (τ) versus r_{apparent} is shown in Figure 7d. This tilt lead to an apparent underestimate of θ and overestimate of D. To correct these quantities for each red cell, the data points in Figure 7d were fitted by the following pragmatic approach. For $0 < r_{\mathrm{apparent}} < 320\,\mu$m the fit function was

$$\mathrm{f}(r_{\mathrm{apparent}}) = \mathrm{a}\, r_{\mathrm{apparent}}^{\mathrm{b}}, \tag{4}$$

with a=2.383 10^{-5} and b=1.648. For $300\,\mu\mathrm{m} < r_{\mathrm{apparent}} < 460\,\mu$m the fit function was

$$\mathrm{g}(r_{\mathrm{apparent}}) = \mathrm{f}(300\,\mu\mathrm{m}) + \mathrm{f}'(300\,\mu\mathrm{m})(r_{\mathrm{apparent}} - 300\,\mu\mathrm{m}) + c(r_{\mathrm{apparent}} - 300\,\mu\mathrm{m})^d, \tag{5}$$

with c=2.699 10^{-8} and d=3.492. The fit is shown in Figure 7d as a continuous line.

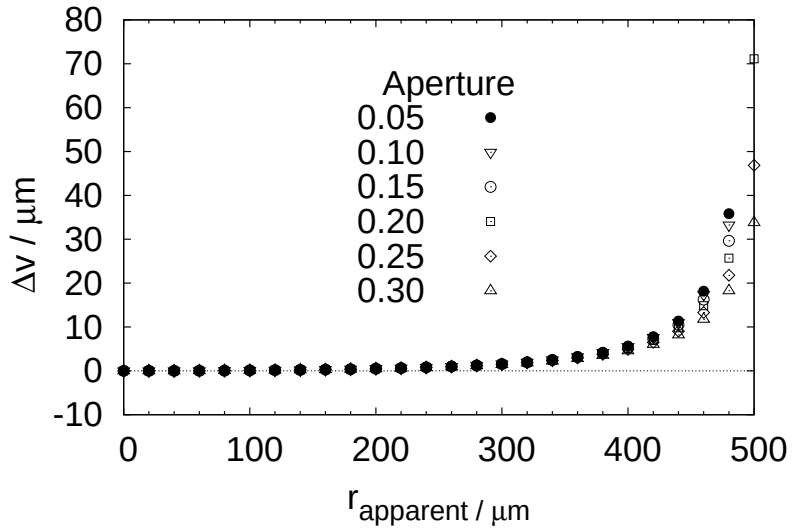

c

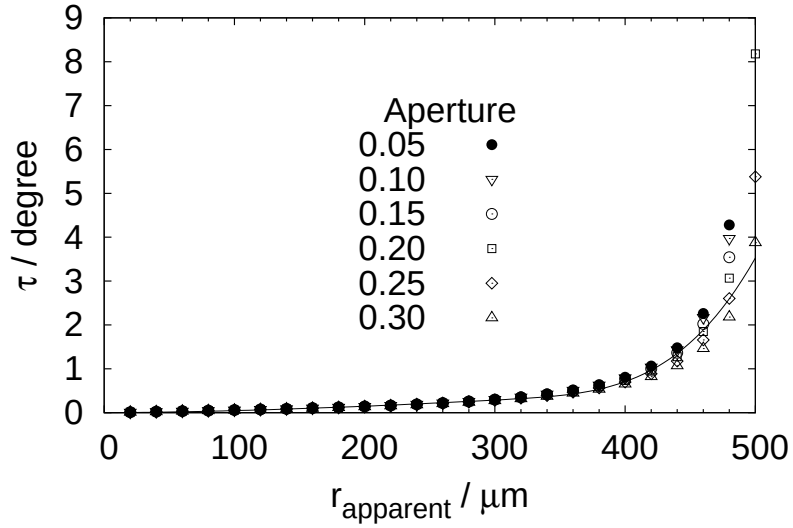

d

Figure 7: Geometric optics calculation for microscopic imaging through a glass capillary embedded in the same liquid which is inside the capillary. The radii were 0.492 and 0.516 mm for the inner and outer radius of the capillary, respectively. The refractive indices were 1.355 and 1.515 for the liquid and glass, respectively. c: Vertical distance (Δv, see Figure 6a) of the focussed red cell from the capillary midplane (green dashed, see Figure 6a) versus the distance of the optical axis from the capillary centerline. d: Tilt angle (τ, see Figure 6a) of the focussed red cell versus the distance of the optical axis from the capillary centerline.

7 Experiments to determine the slip velocity

The slip velocity (v_{slip}) of spheres in Poiseuille flow is given (2) as:

$$v_{\mathrm{slip}} = -\frac{2}{3}\, v_{\mathrm{centerline}} \left(\frac{r_{\mathrm{sphere}}}{R}\right)^2, \tag{6}$$

where R is the luminal radius of the capillary. The fractional deviation of the velocity of a sphere from the velocity of the undisturbed fluid flow at radial position r is:

$$\frac{v_{\mathrm{slip}}}{v_{\mathrm{Poiseuille}}(r)} = -\frac{2}{3}\left(\frac{r_{\mathrm{sphere}}^2}{R^2 - r^2}\right). \tag{7}$$

For a sphere of diameter $2\,\mu$m at $r = 460\,\mu$m, a radial position where wall effects can be considered to be absent, this fractional deviation amounts to 10^{-4}. Therefore the velocity of such latex spheres can be taken as a true indicator of the velocity of the undisturbed fluid flow for $r \leq 460\,\mu$m. For spheres of $8\,\mu$m diameter, the maximum dimension of a resting red cell, the value is 1.6 10^{-3}. This would still be neglegibly small. However, an appreciable deviation was found between the theoretical prediction of solid particles and an observation of tank-treading red cells (3). Because this finding suggested a deviation in behavior of tank-treading red cells compared to solid spheres, experiments were performed to measure the slip velocity of tank-treading red cells in the present geometry.

The capillary was perfused with a suspension of either latex spheres (diameter 2.03 μm) or red cells, both suspended in dextran-salt solutions (14.6 or 55.9 mPas at 23°C). $v_{\mathrm{centerline}}$ ranged from 1.0 to 6.5 mm/s for the 14.6 mPas solution and from 1.2 to 36 mm/s for the 55.9 mPas solution. The flow of latex spheres or red cells was recorded in the radial range from the capillary wall to the centerline. Since small variations in flow could not be excluded, this was done several times for each outflow resistance. For each recording $v_{\mathrm{centerline}}$ was determined by a parabolic fit. All data were normalized by the average of the two encompassing values of $v_{\mathrm{centerline}}$. Only those data were used where the two encompassing values did not differ by more than 2%.

A typical result is shown in Figure 8. It is obvious that there was no difference in velocity between red cells and latex spheres. Had there been a difference, the relative deviation would have been largest at low velocities. Therefore a logarithmic scale was chosen.

8 Determination of the local shear rate

Three parameters are necessary to calculate the shear rate ($\dot{\gamma}$) a flowing particle is subjected to in Poiseuille flow. For the present set up, the following parameters were chosen: the luminal radius of the capillary (R), the radial position (r) and the velocity ($v(r)$) of the flowing particle. The local shear rate is calculated by:

$$\dot{\gamma}(r) = \frac{-2rv(r)}{R^2 - r^2}. \tag{8}$$

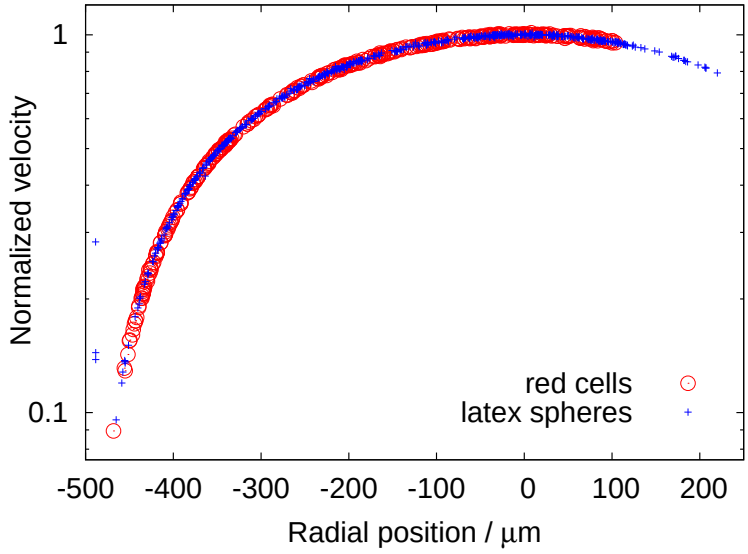

Figure 8: Half logarithmic plot of the normalized velocity distribution of red cells and latex spheres versus the radial position. $v_{\mathrm{centerline}}$ = 1.0 mm/s, viscosity of the suspending phase = 14.6 mPas at 23°C. The points at about $r = 490\,\mu$m result from parts of the image of the capillary wall not completely extinguished by the background correction.

R was determined as described in section 1. For the evaluation of $v(r)$ see section 3. For r we used r_{apparent} (section 6).

References

1. Lindert, J., J. Werner, M. Redlin, H. Kuppe, H. Habazettl, and A. R. Pries, 2002. OPS Imaging of human microcirculation: A short technical report. *JOURNAL OF VASCULAR RESEARCH* 39:368–372.

2. Happel, J., and H. Brenner, 1983. Low Reynolds Number Hydrodynamics. Martinus Nijhoff Publishers, The Hague.

3. Bransky, A., N. Korin, A. Leshansky, N. Lanir, Y. Nemirovski, and U. Dinnar, 2007. The rheologic properties of erythrocytes: a study using an automated rheoscope. *Rheologica Acta* 46:621–627.